Recent Progress in ICRF Experiments on the Experimental Advanced Superconducting Tokamak (EAST)

Wei Zhang [1*], *Ghassan* Antar[2], *Yan* Cheng[1], *Xu* Deng[1], *Songqing* Ju[1], *Yevgen* Kazakov[3], *Lunan* Liu[1], *Yuzhou* Mao[1], *Jozef* Ongena[3], *Chengming* Qin[1], *Lei* Wang[1], *Yongsheng* Wang[1], *Tom* Wouters[4], *Hua* Yang[1], *Shuai* Yuan[1], *Kai* Zhang[1], *Xinjun* Zhang[1], and the EAST team[1]

[1] Institute of Plasma Physics, Chinese Academy of Sciences, Hefei 230031, China
[2] Physics Department, American University of Beirut, Beirut 11072020, Lebanon
[3] Laboratory for Plasma Physics, ERM/KMS, TEC Partner, Brussels 1000, Belgium
[4] ITER Organization, Route de Vinon-sur-Verdon, CS 90 046, 13067 St. Paul Lez Durance Cedex, France

Abstract. Ion Cyclotron Range of Frequency (ICRF) heating is a major auxiliary heating method used on the Experimental Advanced Superconducting Tokamak (EAST). This paper summarizes recent progress in ICRF experiments on EAST, including the upgrade of ICRF heating systems, improvements in ICRF coupling and core RF power absorption, and ICRF heating schemes. Furthermore, ICRF application in multiphysics studies is also discussed, including ICRF-induced Alfvén instabilities, sawtooth control, turbulence suppression, Ion Cyclotron Wall Conditioning (ICWC), and demonstration of good efficiency of ICRF for plasma heating in dominant RF-electron-heated plasmas relevant for ITER. These results demonstrate significant advances in ICRF performance and provide insights into wave–plasma interactions. They offer valuable guidance for improving heating efficiency and plasma control in next-generation fusion devices.

1 Introduction

Plasma heating with waves in the Ion Cyclotron Range of Frequency (ICRF) is widely used in various magnetic confinement fusion devices, including ASDEX-U [1], JET [2, 3], Alcator C-Mod [4], Tore Supra [5], WEST [6, 7], the Experimental Advanced Superconducting Tokamak (EAST) [8], LHD [9] and W7-X [10]. ICRF can directly heat ions and is accessible at a high density. Therefore, it is compatible with future fusion reactors with high plasma densities and large magnetic fields. Consequently, it is considered for future fusion reactors, such as SPARC [11], ITER [12] and CFETR [13].

ICRF is a key heating method for EAST. It is routinely used to obtain long-pulse discharges with excellent plasma parameters. This paper reviews the recent progress in ICRF experiments on EAST. First, recent developments in ICRF systems are introduced, including the application of two new 2-strap antennas and a real-time impedance-matching system. Subsequently, methods for improving ICRF coupling at the plasma edge and core ICRF power absorption are discussed. Finally, ICRF application in multiphysics studies is presented, including Alfvén eigenmode generation, sawtooth suppression, core and edge turbulence suppression, and Ion Cyclotron Wall Conditioning (ICWC). The novel technologies and physics developed in this study can enhance the ICRF heating efficiency and improve plasma parameters in current and future fusion devices.

2 ICRF heating experiments

2.1 The EAST-ICRF system

Two identical 2-strap ICRF antennas were installed on EAST in 2021–2022. The two ICRF antennas are installed in the N- and I-ports. Each antenna is connected to two RF generators, with a coupled power of up to 2.0 MW. Fig. 1 is a schematic representation of the 2-strap antenna as well as the Radio Frequency (RF) generators, impedance matching, and transmission lines. Apart from the 4 MW ICRF power, EAST has approximately 4 MW Lower Hybrid (LH), 6 MW Neutral Beam Injection (NBI), and 3 MW Electron Cyclotron Resonance Heating (ECRH) power.

Comparing the new to the old 2-strap antenna, the former increases the strap distance from 0.225 m to 0.425 m, thereby decreasing the parallel wave number $k_{||}$ from ~13 m^{-1} to ~7.0 m^{-1} [14, 15]. Consequently, the fast-wave cut-off density decreases from ~8×10^{18} m^{-3} to ~2.8×10^{18} m^{-3}, and the coupling resistance increases by a factor of 2–3. The antenna straps, Faraday screen bars, and limiters are actively water-cooled, enabling the antenna to operate in long pulses.

In addition to the antenna upgrades, two high-voltage-tolerant capacitors were installed next to the triple liquid stub tuner on each transmission line. Consequently, this enables fast feedback impedance matching under vacuum

* Corresponding author: zw@ipp.ac.cn

and plasma conditions. Normally, good matching can be achieved within 1 sec by quickly adjusting the motor controller, which can decrease the Voltage Standing Wave Ratio from 5 to less than 1. This enables the high-power and long-pulse operation of the ICRF system.

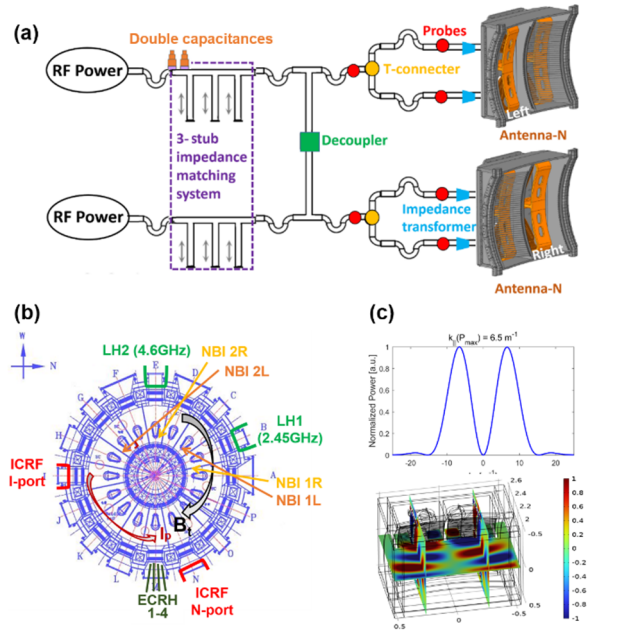

Fig. 1. (a) ICRF heating system, including the RF generator, transmission line, matching system, and antennas; (b) Top view of the auxiliary heating systems; (c) RAPLICASOL simulations of the power spectrum and wave propagation from the antenna.

Fig. 2 illustrates an example of ICRF heating. In the studied discharge, 1.8 MW of ICRF power from the N-port antenna is applied in addition to the 1.3 MW of ECRH and 2.8 MW of LH power. The heating scenario is a hydrogen (H) minority with fundamental resonance. This increases the plasma stored energy by 70 kJ, ion temperature by 0.15 keV, electron temperature by 2.0 keV, and H_{98} factor by 0.36. This indicates the good heating performance of ICRF. Notably, this experiment is performed with a Lithium-coated wall. However, a boron-coated wall will increase the generation of ICRF-specific impurities and degrade the ICRF heating efficiency.

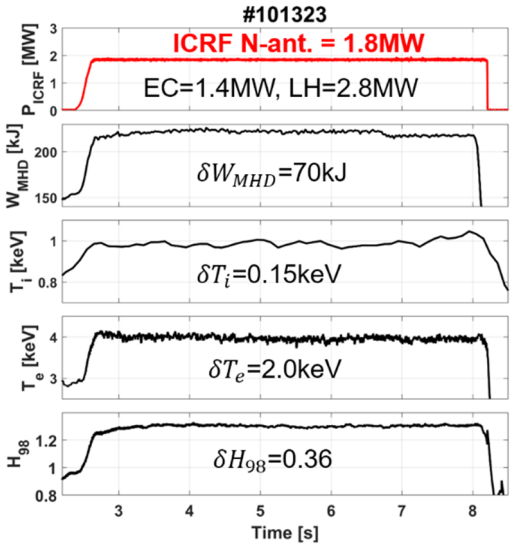

Fig. 2. Example of effective plasma heating with ICRF on EAST with a Lithium-coated wall. The N-port antenna with ICRF power of 1.8 MW is used.

2.2 ICRF coupling and absorption

Efficient ICRF heating depends on the power coupled to the plasma in the scrape-off layer (SOL) and the power absorbed in the plasma core. ICRF coupling can be considerably increased by decreasing the width of the fast-wave evanescent layer and the parallel wave number, which depend on the SOL plasma density and the distance between the current straps, respectively.

Various methods have been attempted on EAST to improve the ICRF coupling by tailoring the SOL density. First, midplane gas puffing close to the antenna increased the coupling resistance by approximately 90% with a moderate gas puff rate of 12e20 el/s. This is in line with the observations from machines such as the ASDEX Upgrade [16-18] and JET [19-21]. Moreover, increasing the global SOL density can also be beneficial for ICRF coupling (Fig. 3) by decreasing the antenna-separatrix distance and increasing the core SOL. Shifting the strike point from the vertical to the horizontal plate in the lower divertor can also increase the SOL density owing to the interplay between divertor closure and plasma drifts, thereby enhancing recycling. Lastly, $(0, \pi)$ phasing is demonstrated as the optimized antenna phasing in ICRF coupling.

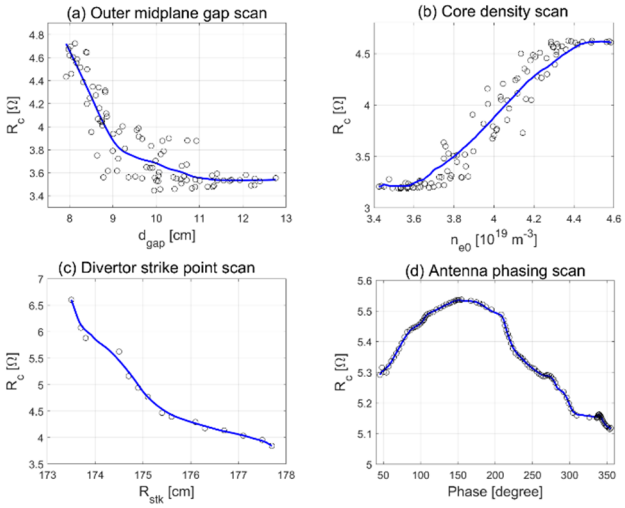

Fig. 3. Dependence of antenna coupling resistance as a function of outer midplane gap (i.e., the width of SOL), core density, divertor strike point, and antenna phasing. The Figure is reproduced with permission from [15].

Hydrogen (H) minority-ion heating is the main heating scenario on EAST. The ICRF power absorption in the plasma core depends on the wave field polarization near the H-cyclotron resonance layer. It can be tuned by the toroidal magnetic field and H minority concentration (X[H]). Experiments were performed by scanning these two parameters. The results indicate that on-axis heating with B_t at ~2.5 T leads to the maximum ICRF power absorption, which worsens as the resonance layer migrates from the magnetic axis. In addition, the ICRF power absorption was the largest when the measured edge X[H] was ~7-10% (Fig. 4), consistent with the results of TORIC simulations.

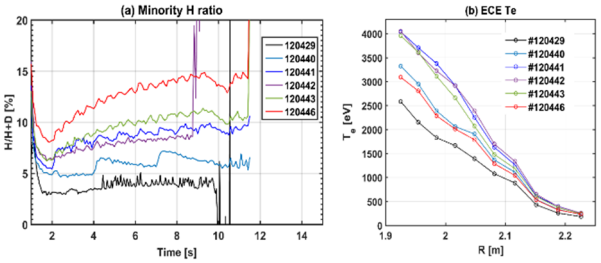

Fig. 4. Influence of Hydrogen minority concentration on ICRF heating and electron temperature. The Figure is reproduced with permission from [15].

2.3 ICRF heating scenarios

In addition to the H minority ion heating, other heating scenarios were evaluated using EAST. One of the most important scenarios is high-harmonic Deuterium (D) heating and its synergetic effects with NBI. The second and third harmonic D heating was achieved with a magnetic field of 2.5 T and 1.7 T, respectively [22, 23]. The injected NBI fast D ions with an energy of approximately 60 keV can be further accelerated by ICRF fields at their harmonics, reaching energies of up to 500 keV. An energetic neutron tail with an energy in the range of 3–7 MeV was also observed owing to the ICRF-NBI synergetic effects. Moreover, both experiments and TRANSP simulations suggest that the synergetic effects of ICRF-NBI can be amplified by changing the minority ion concentration, location of the resonance layer, NBI energy, and injection angle.

The first tests of He^3 minority heating were also carried out on EAST. However, the increase in plasma temperature and stored energy was not as pronounced as with H minority heating, highlighting the need for a better control of ^{3}He minority concentration in future experiments.

In the near future, three-ion heating scenarios, such as the D-(D_{NBI})-^{3}He and D-(^{3}He)-H heating schemes [24, 25], are planned to be tested on EAST. The optimized concentrations for these ICRF scenarios were calculated with TORIC and TOMCAT codes [15].

3 ICRF-related physics studies

3.1 Alfvén instability

The Alfvén Eigenmode (AE) is the most frequently observed plasma instability that can be excited by fast ions. Gradients can drive this instability in either the spatial or velocity distributions. Fig. 5 illustrates the typical AEs with different plasma frequencies, including 158 kHz (n=3), 134 kHz (n=2), and 75 kHz (n=2). Among these three, the previous two are Toroidal Alfvén Eigenmodes (TAEs), which satisfy $f_0 \propto v_A \propto B/\sqrt{\mu_0 n_e}$. Conversely, the third one belongs to Beta-induced Alfvén Eigenmode because it depends on T_e but is independent of n_e. The statistical analysis of the TAE discharges in Li/B-coated walls reveals that the TAEs depend strongly on the H_{98} factor and can only be excited when H_{98} is larger than 1.15. Additionally, a beat wave with a frequency of 100 MHz is also excited because the I- and N-port ICRF antennas use slightly different frequencies of 37.1 MHz and 37.0 MHz.

In parallel with the experiments, integrated simulations with TORIC + ASCOT + NOVA-C were also performed to understand the driving and damping mechanisms of TAE. The driving force mainly originated from the spatial gradient of the fast H-ion distribution. The most accelerated fast H ions have banana orbits with their bouncing tips near the cyclotron resonance layer. D-ion Landau damping is the dominant damping mechanism.

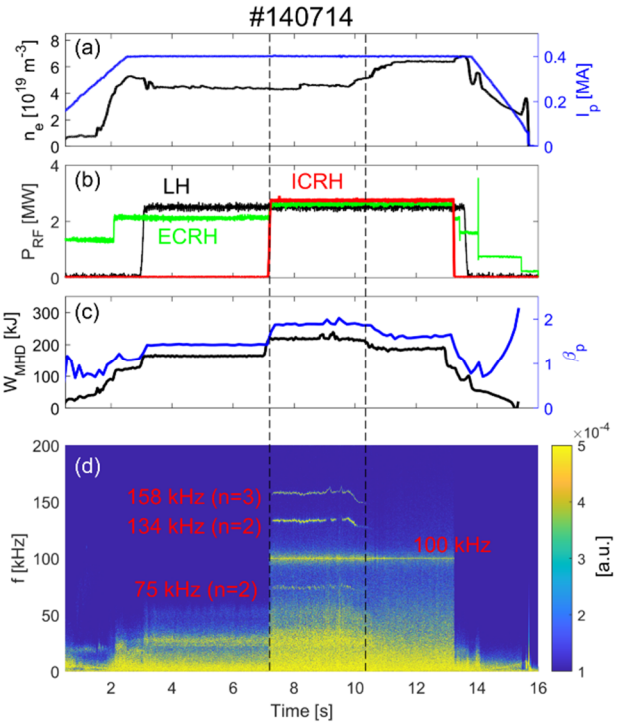

Fig. 5. Excitation of Toroidal Alfvén Eigenmodes and Beta-induced Alfvén Eigenmode by ICRF. The Figure is reproduced with permission from [26].

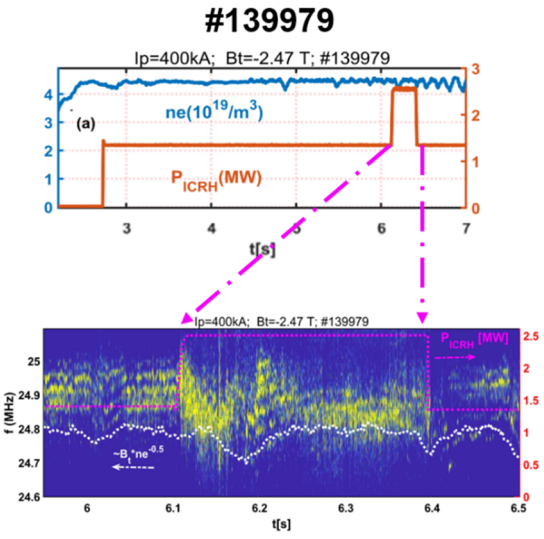

Fig. 6. Excitation of high-frequency AEs (approximately 25 MHz) by ICRF. This Figure is reproduced with permission from [27].

Moreover, high-frequency AEs (of 10 MHz) have also been observed in ICRF-heated plasmas. For instance, Fig. 6 illustrates typical high-frequency AEs of ~25 MHz during ICRF H minority heating. These modes also

correlate with $B/\sqrt{\mu_0 n_e}$, indicating that they are a certain type of AEs. These high-frequency AEs have many harmonic branches that broaden the frequency range (24.8–25 MHz). NBI is not used in this discharge; thus, the fast H-ion is the only driving mechanism. Further analyses are currently underway to understand the excitation of these high-frequency AEs.

3.2 Sawtooth control

A large-period sawtooth can cause larger core plasma perturbations, possibly induce NTMs, and disrupt plasma. In contrast, a small-period sawtooth is often beneficial because it pumps impurities from the plasma core and improves plasma confinement. Two methods were tested on EAST to reduce the period of the sawtooth. One is to modulate the ICRF power by switching between high and low power with a period smaller than the original sawtooth, and the other is to change the ICRF antenna phase.

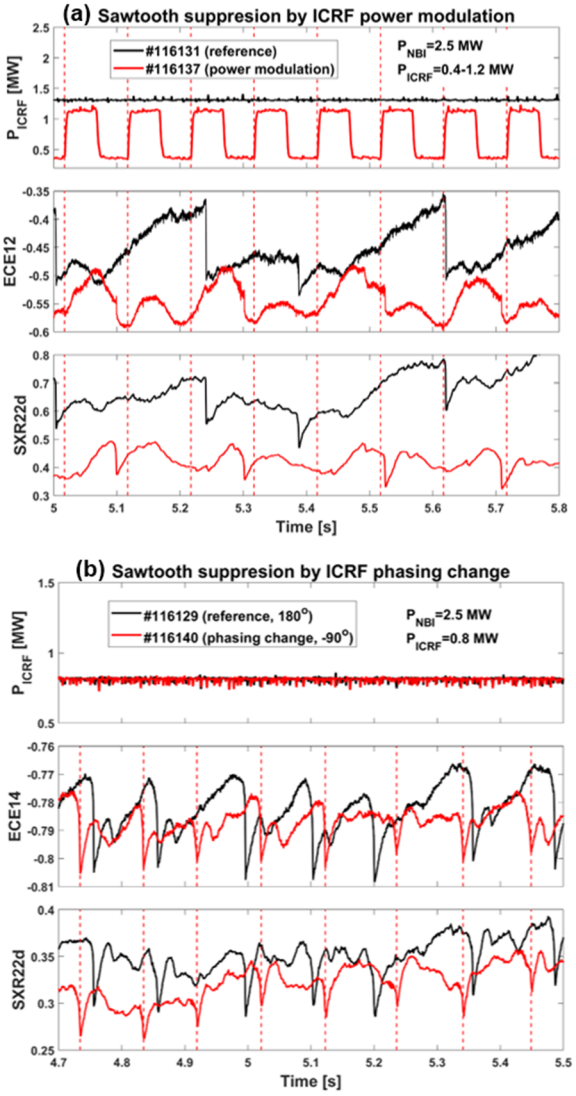

Fig. 7. Sawtooth suppression by ICRF power modulation and phasing change.

As Fig. 7 depicts, ICRF power modulation decreases the sawtooth period from approximately T=0.24 s to 0.1 s, as suggested by the Electron Cyclotron Emission and soft X-ray measurements. Fast-ion measurements reveal that the change in fast-ion pressure inside the q=1 surface is the cause of sawtooth suppression. Changing the antenna phasing from $\Phi = 180^{o}$ (#116129) to $\Phi = -90^{o}$ can also reduce the sawtooth period from approximately T=0.14 s to 0.1 s. Preliminary TRANSP simulations indicate that the change of passing fast ion distribution is the main cause. Further M3D-K simulations are ongoing to understand the change in the fast ion distribution during sawtooth crashes.

3.3 Turbulence suppression

The ICRF can interact with the core and edge turbulence in various forms. The core Doppler Back-Scattering and reflectometry measurements revealed that ICRF can suppress core turbulence. Moreover, the turbulence magnitude decreases as the ICRF power increases. However, this mechanism remains under investigation. It is hypothesized that the fast ions generated by ICRF can suppress ITG/TEM and microinstabilities. The reciprocating Langmuir probe and edge Doppler Back-Scattering measurements uncovered that SOL turbulence can also be suppressed by ICRF, especially for large-scale and low-frequency turbulence. Both experiments and simulations suggest that edge turbulence suppression is attributed to the enhanced poloidal shear flow in the SOL [29]. This shear flow is induced by RF convective cells owing to the inhomogeneity of the RF sheath rectified potential.

3.4 Ion Cyclotron Wall Conditioning (ICWC)

The ICWC is important for plasma discharge cleaning. Previously, two ICRF-cleaning antennas (f = 27 MHz) with low heating power were routinely used for the ICWC [30]. In 2024, the two ICRF heating antennas were used for the ICWC on EAST. The ICWC plasma with heated antennas was brighter than that with cleaned antennas. The D-ICWC is sensitive to the working gas pressure and heating power and requires at least 100 kW to build the plasma. Thus, heating antennas typically use a power of more than 200 kW. When the toroidal magnetic field is increased, the plasma becomes weaker with the D-ICWC discharge using a heating antenna. Boronization was achieved using a D-ICWC with heating antennas.

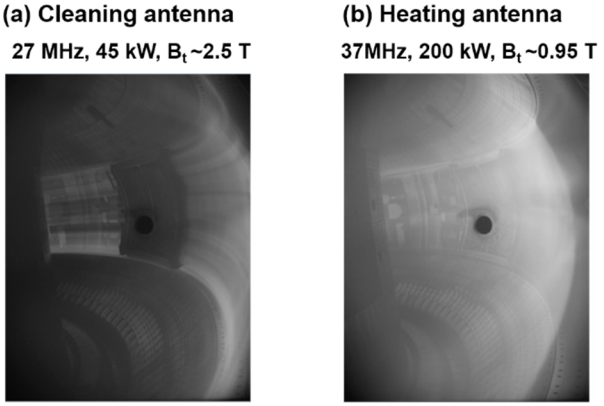

Fig. 8. Comparisons of ICWC with cleaning antenna and heating antenna.

3.5 Optimizing RF plasma mixture in support of the new ITER baseline

The new ITER baseline research plan was published recently [31]. Inter alia, the new baseline foresees the change from beryllium to tungsten as first wall and the modification of the heating mix. The first phase of ITER – start of research operation (SRO) – will include 40 MW of ECRH and 10 MW of ICRH (P_{ICRF}/P_{total} = 20%). The extension of ICRH power to 20 MW is planned for the next DT1 and DT2 phases of ITER operations, subject to successful demonstration of ICRF and its compatibility with full-tungsten environment in SRO.

In support of this development, dedicated experiments were conducted in dominant-electron RF-heated plasmas on EAST with tungsten wall (without lithium coating). The target plasma was set up with 2.6 MW of ECRF and 2.0 MW of LH, resulting in 4.6 MW of RF electron heating, as shown in Fig. 9. Two blips of 1.6 MW of ICRF power (duration 2s each) were applied to demonstrate the compatibility of ICRF under this ITER SRO-relevant conditions (P_{ICRF}/P_{total} ~ 25%). While the tungsten concentration and radiated power increased during the phases with ICRF, the net effect of the application of ICRF power is clearly positive, as seen from the increase of several signals in Fig. 9, including W_{mhd} and T_e. Following previous results and developments presented in Section 2, the ICRF heating scheme adopted in these studies was H minority heating with ~10% hydrogen concentration. For comparison, an identity shot, where the two blips with NBI (instead of ICRF), was performed. The comparison between the two pulses confirms the good efficiency of ICRF for plasma heating in the tungsten plasma on EAST, even in the absence of lithium coating.

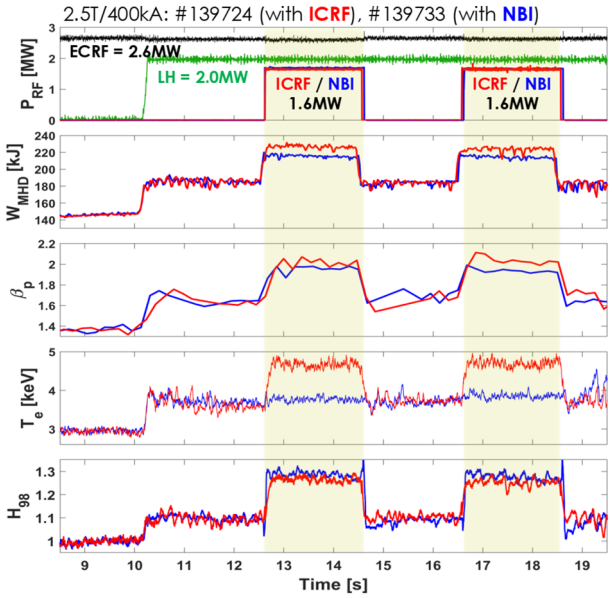

Fig. 9. Comparison of ICRF and NBI heating in dominant RF-electron-heated plasmas relevant for the ITER RSO phase.

4 Conclusions

This paper reviews the recent progress in ICRF experiments on EAST, including the upgrades of the ICRF system, the methods developed to increase ICRF coupling and power absorption, and the development of ICRF heating scenarios. Moreover, ICRF-related multiphysics is also summarized, including ICRF-induced Alfvén instabilities, sawtooth control, turbulence suppression, and ICWC.

Two identical 2-strap antennas with low $k_{\parallel}$ were installed on EAST in 2021–2022. Each antenna could provide up to 2 MW of coupled power. Additionally, capacitances were installed next to the original liquid stub tuners, enabling the heating system to achieve real-time fast impedance matching. After the upgrade, various methods have been developed to enhance ICRF heating efficiency. For instance, ICRF coupling has been improved by local gas puffing, optimization of the gap-out distance, core density, divertor strike-point position, and antenna phasing. The ICRF power absorption was increased by optimizing B_t, X(H). Different heating schemes were assessed in addition to the most frequently used H minority heating scenario, including D second- and third-harmonic heating and He^3 minority heating. Ion-heating scenarios and H high-harmonic heating schemes will also be tested in the near future.

In ICRF-related physics studies, various AEs and ICEs have been observed in plasmas with Lithium or Boron-coated walls. The radial gradient of the fast-ion distribution drives the TAE. Sawtooth suppression manipulation was achieved by ICRF power modulation and ICRF phasing, and the main mechanism was the change in the fast ion pressure and fast ion distribution in the velocity space. ICRF also stabilized the core and edge turbulence. Various poloidal plasma flows produced by ICRF are believed to be the cause. ICRF heating antennas were introduced to obtain ICWC on EAST, and the produced plasma was brighter than that of the specific wall conditioning antenna. Finally, good efficiency of ICRF for plasma heating was demonstrated in dominant RF-electron-heated plasmas, relevant for the ITER RSO phase.

The results presented in this paper can help us to better utilize ICRF to heat the plasma and shed light on solving the key physics to improve plasma confinement in current and future fusion devices.

Acknowledgements

This work was supported by National magnetic confinement fusion energy development research project under grant No. 2022YFE03190200, 2019YFE03070000, by National Natural Science Foundation of China under grant No. 12175273, by the Comprehensive Research Facility for Fusion Technology Program of China under Contract No. 2018-000052-73-01001228, and by the Strategic Priority Research Program of Chinese Academy of Sciences under Grant No. XDB0790203.

References

[1] V. Bobkov et al., ICRF operation with improved antennas in ASDEX Upgrade with W wall, Nuclear Fusion **53**, 093018 (2013). https://doi.org/10.1088/0029-5515/53/9/093018

[2] J. Jacquinot et al., ICRF studies on JET, Plasma Physics and Controlled Fusion **28**, 1-15 (1986). https://doi.org/10.1088/0741-3335/28/1A/002

[3] M. Vrancken et al., Recent ICRF developments at JET, Fusion Engineering and Design **82**, 873-80 (2007). https://doi.org/10.1016/j.fusengdes.2007.05.019

[4] Y. Takase et al., Survey of ICRF heating experiments and enhanced performance modes in Alcator C-Mod, Plasma Physics and Controlled Fusion **38**, 2215-29 (1996). https://doi.org/10.1088/0741-3335/38/12/013

[5] L. Colas et al., Key results of long pulse ICRH operation in Tore Supra, Nuclear Fusion **46**, S500-S13 (2006). https://doi.org/10.1088/0029-5515/46/7/S11

[6] W. Helou et al., Characterizations and first plasma operation of the WEST load-resilient actively cooled ICRF launchers, AIP Conf. Proc. **2254**, 030009 (2020). https://doi.org/10.1063/5.0013992

[7] L. Colas et al., First application of Ion Cyclotron resonant frequency waves on WEST plasma scenarios, AIP Conf. Proc. **2254**, 040004 (2020). https://doi.org/10.1063/5.0013571

[8] X. Zhang et al., Main experimental results and challenges in ICRF heating on EAST, Main experimental results and challenges in ICRF heating on EAST, AIP Conf. Proc. **2254**, 030004 (2020). https://doi.org/10.1063/5.0013587

[9] K. Saito et al., Ion and electron heating in ICRF heating experiments on LHD, Nuclear Fusion **41**, 1021-35 (2001). https://doi.org/10.1088/0029-5515/41/8/306

[10] J. Ongena et al., Physics design, construction and commissioning of the ICRH system for the stellarator Wendelstein 7-X, Fusion Engineering and Design **192**, 113627 (2023). https://doi.org/10.1016/j.fusengdes.2023.113627

[11] Y. Lin et al., Physics basis for the ICRF system of the SPARC tokamak, Journal of Plasma Physics **86**, 865860506 (2020). https://doi.org/10.1017/S0022377820001269

[12] P. Lamalle et al., Status of the ITER ion cyclotron heating and current drive system, AIP Conf. Proc. **1689**, 030007 (2015). https://doi.org/10.1063/1.4936472

[13] J. Li et al., Present State of Chinese Magnetic Fusion Development and Future Plans, Journal of Fusion Energy **38**, 113-24 (2019). https://doi.org/10.1007/s10894-018-0165-2

[14] X. J. Zhang et al., First experimental results with new ICRF antenna in EAST, Nuclear Fusion **62**, 086038 (2022). https://doi.org/10.1088/1741-4326/ac7657

[15] W. Zhang et al., Recent progress in improvement in ion cyclotron range of frequencies coupling and power absorption with new antennas of Experimental Advanced Superconducting Tokamak (EAST), Nuclear Fusion **64**, 096011 (2024). https://doi.org/10.1088/1741-4326/ad63bb

[16] P. Jacquet et al., Improvement of ICRF antenna loading by local gas injection on ASDEX Upgrade, Nuclear Fusion **52**, 042002 (2012). https://doi.org/10.1088/0029-5515/52/4/042002

[17] V. Bobkov et al., Influence of gas injection location and magnetic perturbations on ICRF antenna performance in ASDEX Upgrade, AIP Conf. Proc. **1580**, 271 (2014). https://doi.org/10.1063/1.4864540

[18] W. Zhang et al., 3D simulations of gas puff effects on edge density and ICRF coupling in ASDEX Upgrade, Nuclear Fusion **56**, 036007 (2016). https://doi.org/10.1088/0029-5515/56/3/036007

[19] E. Lerche et al., Impact of localized gas injection on ICRF coupling and SOL parameters in JET-ILW H-mode plasmas, Journal of Nuclear Materials **463**, 634-9 (2015). https://doi.org/10.1016/j.jnucmat.2014.10.074

[20] P. Jacquet et al., Maximization of ICRF power by SOL density tailoring with local gas injection, Nuclear Fusion **56**, 046001 (2016). https://doi.org/10.1088/0029-5515/56/4/046001

[21] W. Zhang et al., 3D simulations of gas puff effects on edge plasma and ICRF coupling in JET, Nuclear Fusion **57**, 056042 (2017). https://doi.org/10.1088/1741-4326/aa6817

[22] W. Zhang et al., Parametric study of midplane gas puffing to maximize ICRF power coupling in ITER, Nuclear Fusion **63**, 056015 (2023). https://doi.org/10.1088/1741-4326/acb4ad

[23] G. Zhu et al., First results from third harmonic ion cyclotron acceleration of deuterium beams in EAST ion heating studies experiments, Nuclear Fusion **63**, 036013 (2023). https://doi.org/10.1088/1741-4326/acb2dc

[24] Y. O. Kazakov et al., Efficient generation of energetic ions in multi-ion plasmas by radio-frequency heating, Nature Physics **13**, 973 (2017). http://doi.org/10.1038/nphys4167

[25] Y. O. Kazakov et al., Physics and applications of three-ion ICRF scenarios for fusion research, Physics of Plasmas **28**, 020501 (2021). https://doi.org/10.1063/5.0021818

[26] W. Zhang, Stability analysis of Alfvén eigenmodes excited by ion cyclotron resonance heating on EAST, submitted to Plasma Physics and Controlled Fusion, 2025

[27] L. Liu et al., Observation of high frequency Alfvén eigenmodes excited by RF-accelerated minority hydrogen ions in the EAST tokamak, Nuclear Fusion **64**, 124002 (2024). https://doi.org/10.1088/1741-4326/ad83e2

[28] Z. S. Y. Wang, Experimental and numerical investigation of sawtooth suppression by ICRF on EAST, to be submitted to Nuclear Fusion, 2025

[29] W. Zhang et al., Experimental and numerical investigation of ICRF induced low-frequency turbulence reduction across the scrape-off layer on the EAST tokamak, Physics of Plasmas **31**, 032502 (2024). https://doi.org/10.1063/5.0192870

[30] Y. Yu et al., ICRF (ion cyclotron range of frequencies) discharge cleaning with toroidal and vertical fields on EAST, Plasma Physics and Controlled Fusion **53**, 015013 (2011). https://doi.org/10.1088/0741-3335/53/1/015013

[31] A. Loarte et al., The new ITER baseline, research plan and open R&D issues, Plasma Physics and Controlled Fusion **67**, 065023 (2025). https://doi.org/10.1088/1361-6587/add9c9